PHYSICAL REVIEW D **96,** 036001 (2017)

Radiative corrections to false vacuum decay in quantum mechanics

M. A. Bezuglov[1,2] and A. I. Onishchenko[1,2,3]

[1]*Bogoliubov Laboratory of Theoretical Physics, Joint Institute for Nuclear Research, Joliot-Curie 6, 141980 Dubna, Moscow region, Russia*

[2]*Moscow Institute of Physics and Technology (State University), 9 Institutskiy per., 141701 Dolgoprudny, Moscow Region, Russian Federation*

[3]*Skobeltsyn Institute of Nuclear Physics, Moscow State University, 1(2), Leninskie gory, GSP-1, 119991 Moscow, Russian Federation*

(Received 17 June 2017; published 2 August 2017)

We consider radiative corrections to false vacuum decay within the framework of quantum mechanics for the general potential of the form $\frac{1}{2}M\phi^2(\phi - A)(\phi - B)$, where M, A and B are arbitrary parameters. For this type of potential we provide analytical results for Green function in the background of a corresponding bounce solution together with a one loop expression for false vacuum decay rate. Next, we discuss the computations of higher order corrections for false vacuum decay rates and provide numerical expressions for two and three loop contributions.

DOI: 10.1103/PhysRevD.96.036001

I. INTRODUCTION

First-order phase transitions driven by scalar fields play an important role in high-energy, astro-particle physics and cosmology. Such first order phase transitions go through the nucleation of new phase bubbles, often around impurities, which subsequently expand. A well known example, which attracted recently a lot of attention, is the possible metastability[1] of an electroweak vacuum at a scale around 10^{11} GeV [10–17]. Next, first-order phase transitions have a potential of producing stochastic gravitational wave backgrounds [18–22], which could be further studied experimentally by existing and forthcoming gravitational wave experiments [23]. In addition, first order electroweak phase transition may satisfy Sakharov's conditions [24] and be responsible for the generation of the baryon asymmetry of our Universe, see [25,26] and references therein. The amount of produced baryon asymmetry crucially depends on the dynamics of phase transition. It should be noted, that in Standard Model the electroweak phase transition is not actually first order, but a crossover [27–30]. However, electroweak baryogenesis could survive in its extensions, many of which include extra dynamical scalar fields. The role of impurities catalyzing the mentioned first-order phase transitions may be played by small evaporating black holes or other gravitational inhomogeneities, see [31–34] and references therein.

The first rigorous description of the mentioned quantum phase transition between different vacuum states appeared in [35–38]. As is known, the false vacuum decay rate may be related to the imaginary part of ground state energy. However, to calculate the latter one first needs to perform an analytical continuation of the potential so that the false vacuum is stable. This original method was further developed and is known now as the *potential deformation method*, see for review [39–44]. Recently a more direct way to compute tunneling probabilities using path integrals appeared in [45], see also [44]. In both methods the decay rates are given by path integrals around bounce configurations (solutions of the Euclidean equations of motion used to evaluate path integrals in saddle point approximation) divided by corresponding path integrals around static false vacuum (FV) solutions.

At one loop there is a number of different methods to compute functional determinants arising in the evaluation of path integrals. Among them are direct evaluations of spectrum for solvable potentials,[2] heat kernel methods [46–49], Green function methods [50–54], and of course, the famous Gel'fand-Yaglom method [55] and its generalizations [56,57]. The methods beyond one loop were mostly developed in the study of instantons [58–60] in quantum mechanics [61–65], the effective Euler-Heisenberg Lagrangian [66–68], and corrections to classical string solutions [69,70].

The purpose of this paper is to extend the methods of [61–65] for the computation of higher order radiative corrections to false vacuum decay in quantum mechanics. We organized the paper as follows. In Sec. II we set up our framework and present bounce solutions for the potential of the most general form containing both cubic and quartic interactions. Next, we derive analytical expressions for the Green function in the background of the found bounce solution. We were able to determine the one-loop false vacuum decay rate analytically using the Gel'fand-Yaglom method. Beyond the one loop, we used the Feynman diagram technique on the top of false vacuum and bounce solutions to get two and three loop corrections to the decay rate. Finally, in Sec. III we come with our conclusion.

[1]For tunneling rates calculations in the Standard Model and its extensions, see [1–9] and references therein.

[2]See [42] and references therein.

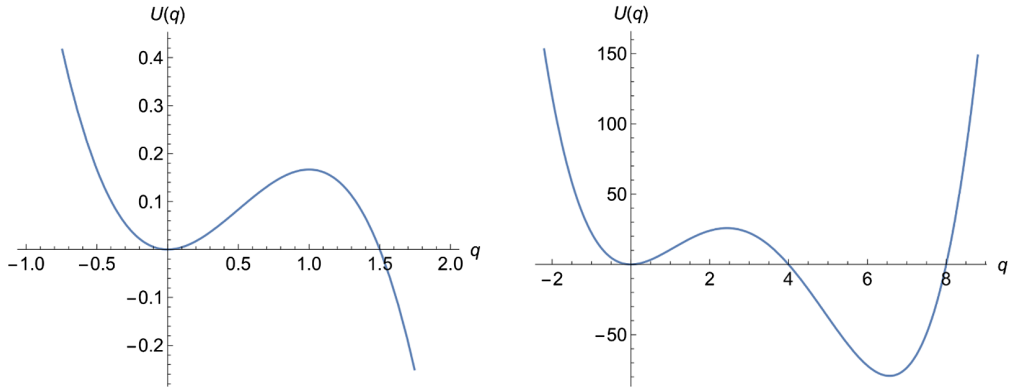

FIG. 1. The potentials for two specific choices of parameters, $U(q) = \frac{1}{2}q^2 - \frac{1}{3}q^3$ on the left and $U(q) = \frac{1}{2}q^2(q-4)(q-8)$ on the right.

II. FALSE VACUUM DECAY IN QUANTUM MECHANICS

The perturbative vacuum obtained by small quantum fluctuations around a false (metastable) vacuum will eventually decay. This means that the energy of the ground state has a small imaginary part. The most convenient way to compute ground state energy is to consider small temperature behavior of the thermal partition function.

$$Z(\beta) = \mathrm{tr} e^{-\beta H(\beta)}, \tag{1}$$

so that

$$E = -\lim_{\beta\to\infty} \frac{1}{\beta} \log Z(\beta). \tag{2}$$

The imaginary part of the energy comes from imaginary part of the thermal partition function[3]

$$\mathrm{Im}E = -\lim_{\beta\to\infty} \frac{1}{\beta} \frac{\mathrm{Im}Z}{\mathrm{Re}Z}. \tag{3}$$

To compute thermal partition function $Z(\beta)$ we will use its path integral representation

$$Z(\beta) = \int \mathcal{D}[q(t)] e^{-S(q)}, \tag{4}$$

where the Euclidean action $S(q)$ is given by

$$S(q) = \int_{-\beta/2}^{\beta/2} dt \left[\frac{1}{2}(\dot{q}(t))^2 + U(q)\right], \tag{5}$$

and the path integral is taken over periodic trajectories, such that

$$q(-\beta/2) = q(\beta/2). \tag{6}$$

[3]See for example [42].

We will be interested in the general potential of the form

$$U(q) = \frac{1}{2}Mq^2(q-A)(q-B) = \frac{m}{2}q^2 + \frac{a}{3}q^3 + \frac{b}{4}q^4, \tag{7}$$

where M, A and B (m, a and b) are arbitrary parameters, such that M, A $B > 0$ ($m > 0$, $a < 0$, $b > 0$). The two sets of parameters M, A, B and m, a, b are related to each other via

$$M = \frac{b}{2}, \qquad A = \frac{-2a}{3b}\left(1 - \sqrt{1 - \frac{9bm}{2a^2}}\right),$$
$$B = \frac{-2a}{3b}\left(1 + \sqrt{1 - \frac{9bm}{2a^2}}\right). \tag{8}$$

This particular potential is the most general potential having qubic and quartic interaction terms in addition to the harmonic potential. The typical potentials generally considered in literature arise as its limiting cases. At the same time, this particular potential is amenable to analytical treatment similar to the well-known case of double well potential. In Fig. 1 we plotted the potential for two specific choices of parameters.

As we already mentioned in the Introduction, the real part of the thermal partition function is given by the path integral around a false vacuum, while the imaginary part is given by the path integral around a bounce solution.[4] The bounce solution is the solution of the classical equation of motion connecting the minima of the potential, which could be easily found using energy conservation for the inverted potential $V(q) = -U(q)$:

$$\frac{1}{2}\dot{q}^2 - U(q) = 0 = E(\beta \to \infty), \tag{9}$$

where we have stressed that we are looking for the $\beta = \infty$ solution corresponding to classical false vacuum energy.

[4]We refer interested reader for example to [44] for more details.

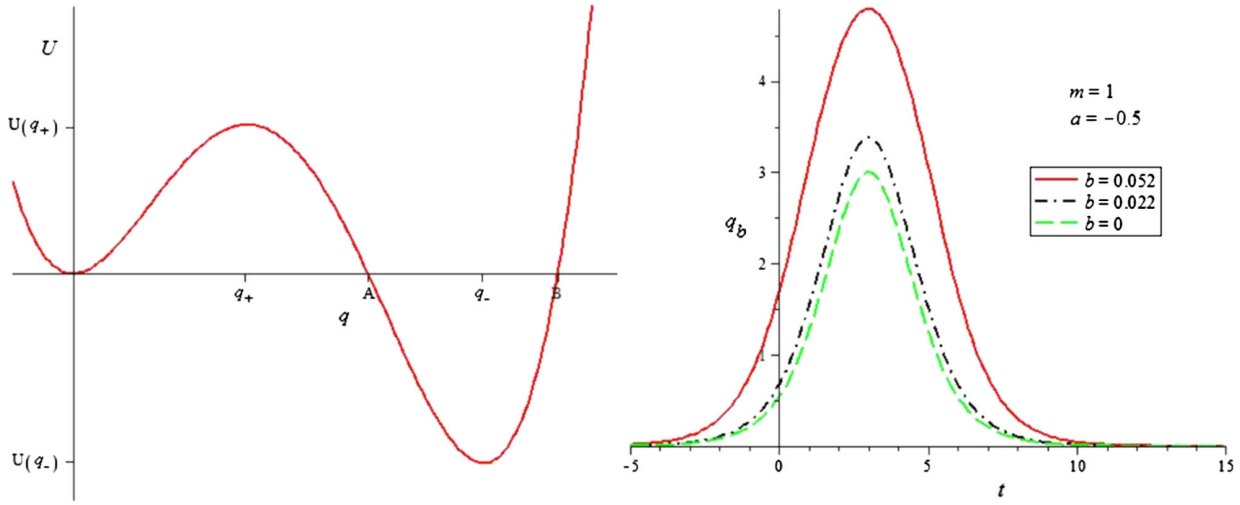

FIG. 2. $U(q)$ on the left and corresponding bounce solution on the right.

Integrating the above energy conservation condition, we get the mentioned bounce solution parameterized by t_0

$$q_b(t) = \frac{2AB}{A + B + (B - A)\cosh(\sqrt{ABM}(t - t_0))}. \quad (10)$$

Figure 2 contains an example of a bounce solution in the limit of small b, where $U(q_\pm)$ and $q_\pm$ are given by

$$U(q_\pm) = \frac{-1}{24b^3}\left(a^4 - 6a^2bm + 6b^2m^2 \mp \mp a^4\left(1 - \frac{4bm}{a^2}\right)^{\frac{3}{2}}\right) \quad (11)$$

$$q_\pm = -\frac{a}{2b}\left(1 \mp \sqrt{1 - \frac{4bm}{a^2}}\right). \quad (12)$$

Next, the bounce action is independent of t_0 and is given by

$$S_b = \frac{1}{12}\sqrt{M}\left\{\sqrt{AB}(3A^2 - 2AB + 3B^2) - 3(A - B)^2(A + B)arc\tan h\left(\frac{\sqrt{A}}{\sqrt{B}}\right)\right\}, \quad (13)$$

where $arc\tan h(x) = \frac{1}{2}\log\frac{1+x}{1-x}$. The original action (5) may be further rewritten in terms of the deviation from the classical configuration, $\varphi(t) \equiv q(t) - q_b(t)$ as

$$S = S_b + \frac{1}{2}\int_{-\beta/2}^{\beta/2} dt\varphi(t)\mathbb{D}\varphi(t) + \int_{-\beta/2}^{\beta/2} dt\left(\frac{4ABM}{A + B + (B - A)\cosh(T)} - \frac{1}{2}M(A + B)\right)\varphi^3(t) + \frac{1}{2}M\int_{-\beta/2}^{\beta/2} dt\varphi^4(t), \quad (14)$$

where

$$\mathbb{D} \equiv -\frac{d^2}{dt^2} + ABM\left[1 - \frac{6B}{A + B + (B - A)\cosh(T)} + \frac{6A((A - B)\cosh(T) - A + 3B)}{(A + B + (B - A)\cosh(T))^2}\right], \quad (15)$$

and we have introduced the abbreviation $T = \sqrt{ABM}t$. While making the transition to the deviations from the bounce solution, special care should be taken due to the existence of the zero mode of operator $\mathbb{D}$. The latter is given by $\varphi_0(t) = -S_b^{-1/2}\frac{d}{dt_0}q_b(t)$. To integrate over this zero mode, we employ a Faddeev-Popov-like trick, as in [61,62], and insert the unity operator into our path integral, written as[5]

$$1 = \int dt_0\delta(f(t_0))\frac{df(t_0)}{dt_0}, \quad (16)$$

[5]See also [59,60].

where

$$f(t_0) = \int \varphi(\tau)\varphi_0(\tau)d\tau = \int (q(\tau) - q_b(\tau))\varphi_0(\tau)d\tau, \tag{17}$$

$$\frac{df(t_0)}{dt_0} = S_b^{1/2} + \int \varphi(\tau)\frac{d}{dt_0}\varphi_0(\tau)d\tau. \tag{18}$$

This way we get

$$1 = \int dt_0 \left(S_b^{1/2} + \int \varphi(\tau)\frac{d}{dt_0}\varphi_0(\tau)d\tau \right)\delta(c_0), \tag{19}$$

where c_0 is the coefficient in front of our zero mode in the expansion of deviation $\varphi(\tau)$ in terms of eigenfunctions of the $\mathbb{D}$ operator

$$\varphi(\tau) = \sum_n c_n \varphi_n(\tau). \tag{20}$$

We see, that this procedure gives us an extra tadpole vertex coming from the integration measure in addition to those we get from the Lagrangian (14). The presented procedure is known as a transition to collective coordinates. In the case under consideration, the only collective coordinate present is given by t_0.

A. Green function in the background of a bounce solution

The Green function at a false vacuum is easy to find, and it is given by the solution of corresponding Schrödinger equation:

$$G_{FV}(t_1, t_2) = \frac{1}{2\sqrt{ABM}}\exp^{-\sqrt{ABM}|t_1 - t_2|} \tag{21}$$

or

$$G_{FV}(x, y) = \frac{1}{2\sqrt{ABM}}\frac{1 - |x - y| - xy}{1 + |x - y| - xy}, \tag{22}$$

where $x = \tanh\frac{\sqrt{ABM}t_1}{2}$ and $y = \tanh\frac{\sqrt{ABM}t_2}{2}$.

The determination of the Green function in the background of a bounce solution is more involved. As we have already seen in the previous section, the corresponding inverse operator $\mathbb{D}$ has a zero mode. The inversion of the latter is consistently defined only on the subspace of functions orthogonal to this zero mode (Fredholm alternative). More concretely, the Green function we will be looking for is defined as[6]

$$G_b(t_1, t_2) = \sum_{n,\lambda_n \neq 0} \frac{\varphi_n(t_1)\varphi_n(t_2)}{\lambda_n}, \tag{23}$$

where $\mathbb{D}\varphi_n = \lambda_n\varphi_n$ and the summation goes over all modes except the zero one. It is easy to check that the equation satisfied by this Green function is given by

$$\mathbb{D}G_b(t_1, t_2) = \delta(t_1 - t_2) - \varphi_0(t_1)\varphi_0(t_2) \tag{24}$$

or

$$\frac{\partial}{\partial x}\left((1 - x^2)\frac{\partial G_b(x, y)}{\partial x}\right) - \frac{4\{r^4x^2(3 - 2x^2) + r^2(3x^4 - 8x^2 + 3) + (3x^2 - 2)\}}{(1 - x^2)(1 - r^2x^2)^2}G_b(x, y)$$
$$= -\frac{2}{\sqrt{ABM}}\delta(x - y) + \frac{\gamma xy(1 - y^2)}{(1 - r^2x^2)^2(1 - r^2y^2)^2}, \tag{25}$$

where $r = \sqrt{\frac{A}{B}}$ and

$$\gamma = \frac{1}{\sqrt{ABM}} \times \frac{48r^5(1 - r^2)^2}{r(3 - 2r^2 + 3r^4) - 3(1 - r^2)^2(1 + r^2)\tanh^{-1}(r)}. \tag{26}$$

The first solution of the homogeneous equation is given by the zero mode of the operator $\mathbb{D}$ we found in the previous section:

$$y_{hom,1}(x) = \frac{x(1 - x^2)}{(1 - r^2x^2)^2}. \tag{27}$$

The second solution may be found using the so-called reduction of order method. First, from Abel's differential equation identity, we get an equation for the Wronskian of homogeneous solutions $W(x) \equiv y_{hom,1}(x)y'_{hom,2}(x) - y'_{hom,1}(x)y_{hom,2}(x)$:

$$\frac{dW(x)}{W(x)} = -d\log(1 - x^2). \tag{28}$$

Integrating the latter together with the subsequent first order differential equation (obtained from known expressions for Wronskian and first homogeneous solution) for $y_{hom,2}(x)$, we get

[6]The normalization of wave functions to unity is assumed.

$$y_{hom,2}(x) = y_{hom,1}(x)\int \frac{dx}{(1-x^2)y_{hom,1}^2(x)}$$
$$= \frac{x(1-x^2)}{16(1-r^2x^2)^2}\left\{-\frac{16}{x} - 16r^8x + \frac{4x(1-r^2)^4}{(1-x^2)^2} + \frac{2(1-r^2)^3(7+9r^2)x}{1-x^2} + 3(1-r^2)^2(5+6r^2+5r^4)\log\frac{1+x}{1-x}\right\}.$$

The particular solution of the nonhomogeneous solution is then found by the variation of constants and is given by

$$y_{\text{nonhom}}(x) = y_{hom,2}(x)\int \frac{y_{hom,1}(x)f(x)}{W(x)}dx - y_{hom,1}(x)\int \frac{y_{hom,2}(x)f(x)}{W(x)}dx, \tag{29}$$

where

$$f(x) = \frac{\gamma xy(1-y^2)}{(1-x^2)(1-r^2x^2)^2(1-r^2y^2)^2}. \tag{30}$$

The integrals in the above expression could be evaluated in terms of polylogarithms. However, the expressions we get are quite lengthy, and we put them in the mathematica file accompanying this article (see Supplemental Material [71]). Here, we will present analytical expressions only for two particular cases. In the limit[7] $b \to 0$ we get

$$y_{\text{nonhom}}(x,y) = \frac{3xy(1-y^2)}{4}\left(1 + \frac{1}{3(1-x^2)}\right) \tag{31}$$

and in the case $r = \sqrt{\frac{A}{B}} = \frac{1}{\sqrt{2}}$ the particular solution takes the form:

$$y_{\text{nonhom}}(x,y) = y_0(x,y)\left\{\frac{183-89x^2-72x^4}{96(x^2-1)^2} - \frac{37}{256}(44+9\sqrt{2}\log(3-2\sqrt{2}))\log(1-x) + \frac{37}{256}(-44+9\sqrt{2}\log(3+2\sqrt{2}))\log(1+x) + \frac{407}{64}\log(2-x^2) - \frac{3(128-273x^2+135x^4+8x^6)}{64\sqrt{2}x(x^2-1)^2}\log\left(\frac{2-\sqrt{2}x}{2+\sqrt{2}x}\right) + 2\log\left(\frac{x^2-1}{x^2-2}\right) - \frac{333}{128\sqrt{2}}[\text{Li}_2((1-\sqrt{2})(x-1)) - \text{Li}_2((1+\sqrt{2})(x-1)) + \text{Li}_2((\sqrt{2}-1)(1+x)) - \text{Li}_2(-(1+\sqrt{2})(1+x))]\right\}, \tag{32}$$

where

$$y_0(x,y) = \frac{\gamma|_{r=1/\sqrt{2}}xy(1-x^2)(1-y^2)}{(2-x^2)^2(2-y^2)^2}. \tag{33}$$

The Green function in the background of the bounce solution is then given by

$$G(x,y) = C_1(y)y_{hom,1}(x) + C_2(y)y_{hom,2}(x) + y_{\text{nonhom}}(x,y), \tag{34}$$

with $C_1(y)$ and $C_2(y)$, which are some arbitrary functions of variable y. The latter are determined from the conditions:

(1) $G(x,y)$ is finite for $x \to \pm 1$ ($t_1 \to \pm\infty$);
(2) $G(x,y)$ is continuous at $x = y$ ($t_1 = t_2$);
(3) $G(x,y)$ is orthogonal to the zero mode $y_{hom,1}(x)$ (27) (we accounted for the Jacobian of transition from t_1 to x, $J = \frac{2}{1-x^2}$):

$$\int_{-1}^{1}\frac{dx}{1-x^2}y_{hom,1}(x)G(x,y) = 0. \tag{35}$$

Using the first two conditions together with the fact that the Green function is symmetric with respect to the

[7]One should take a limit and not just set b to zero.

exchange of variables $x \leftrightarrow y$, we were able to determine the Green function analytically up to one unknown constant. The latter could be found using the third condition numerically. The resulting expression for the Green function is too lengthy and could be found in the accompanying mathematica file. In the limit $b \to 0$, the analytical expression is quite short and the corresponding Green function is given by ($\frac{bm}{a^2} \ll 1$ or $\frac{A}{B} \ll 1$)

$$G(x,y) = G_0(x,y) + bG_1(x,y) + \mathcal{O}(b^2), \tag{36}$$

where

$$G_0(x,y) = \frac{1}{2m^{1/2}}\left[g_0(x,y)\left[(x^2+y^2)(6xy-4) + 3xy(4-5xy) - \frac{1}{4}|x-y|(8-55xy+15x^2y^2+8(x^2+y^2))\right] + \frac{15}{8}xy(1-x^2)(1-y^2)\left(\log\left(g_0(x,y)\right) - \frac{31}{15}\right)\right], \tag{37}$$

$$G_1(x,y) = \frac{9m^{1/2}}{16a^2}\left[3xy(x^2+y^2-x^4-y^4) - xy\left(\frac{(1-y^2)^2}{1-x^2} + \frac{(1-x^2)^2}{1-y^2}\right) + \frac{|x-y|}{2}\left\{xy(6-5(x^2+y^2)) + +26x^2y^2 - 10(x^2+y^2-x^4-y^4) - 15x^2y^2(x^2+y^2) + 2(x+y)\left(\frac{x(1-x^2)}{1-y^2} + \frac{y(1-y^2)}{1-x^2}\right)\right\} + \frac{3}{28}xy(1-x^2)(1-y^2)\left\{35(x^2+y^2)\left(\log\left(g_0(x,y)\right) - \frac{217}{105}\right) - 30\log(1-|x-y|-xy) - 2\log(1+|x-y|-xy) - \frac{242}{5} + 64\log 2\right\}\right]$$

and

$$g_0(x,y) = \frac{1-|x-y|-xy}{1+|x-y|-xy}. \tag{38}$$

Finally, Figs. 3 and 4 contain plots of Green functions in the background of the bounce solution for two sets of parameters $m = 1$, $b = 0$ and $M = 1$, $A = 4$, $B = 8$.

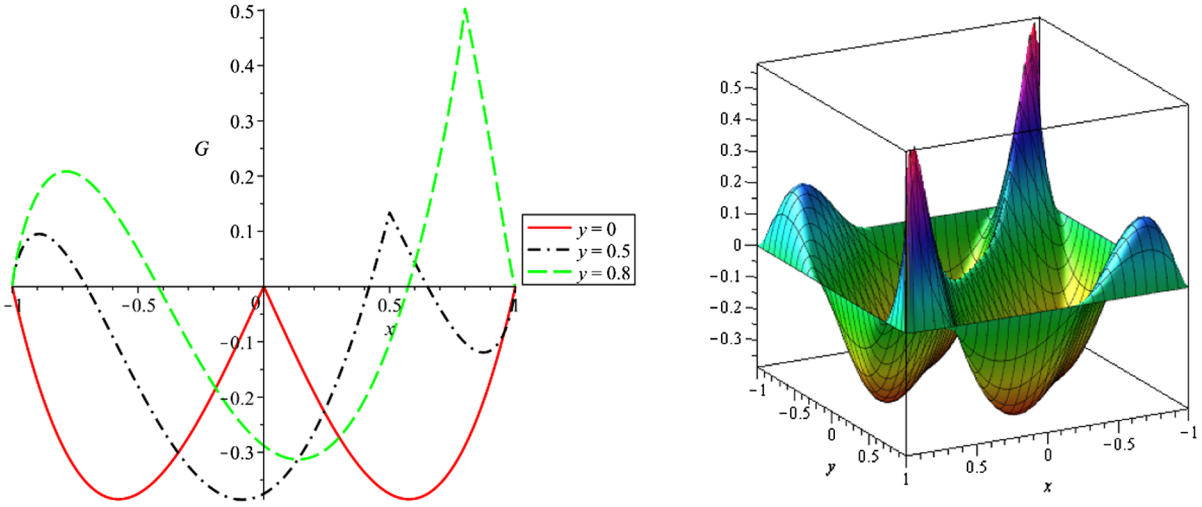

FIG. 3. The Green function in the background of the bounce solution for $m = 1$, $b = 0$: (left)—values of Green function at $y = 0$ (solid line), $y = 0.5$ (dot-dashed line), $y = 0.8$ (dashed line), (right)—the Green function as a function of x, y variables

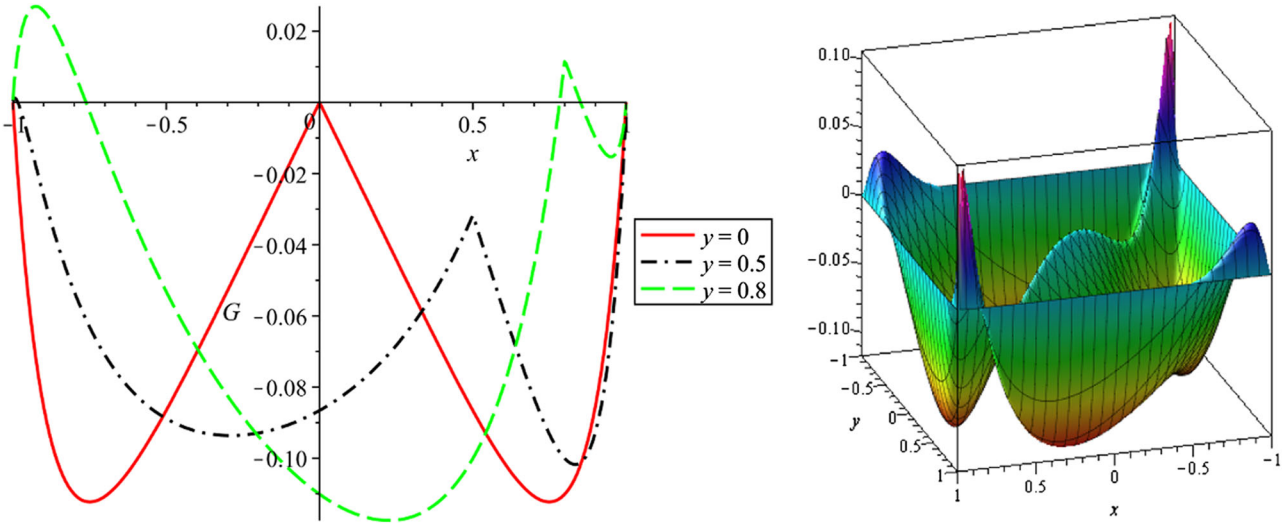

FIG. 4. Green function in the background of bounce solution for $M = 1$, $A = 4$, $B = 8$: (left)—values of Green function at $y = 0$ (solid line), $y = 0.5$ (dot-dashed line), $y = 0.8$ (dashed line), (right)—Green function as a function of x, y variables

B. One loop expression

At one loop, the real and imaginary parts of our thermal partition function are given by[8] (Z_{FV} is the partition function evaluated by the expansion at false vacuum):

$$\mathrm{Re}Z = Z_{FV}(\beta) \tag{39}$$

$$\mathrm{Im}Z = \frac{1}{2i} Z_{FV}(\beta) \lim_{\beta\to\infty} \left[-\frac{\det'\mathbb{D}}{\det \mathbb{D}_{FV}}\right]^{-1/2} \frac{\beta S_b^{1/2}}{\sqrt{2\pi}} e^{-S_b} \tag{40}$$

so, that for imaginary part of energy we get

$$\mathrm{Im}E = \frac{S_b^{1/2}}{2\sqrt{2\pi}} \lim_{\beta\to\infty} \left[-\frac{\det'\mathbb{D}}{\det \mathbb{D}_{FV}}\right]^{-1/2} e^{-S_b}. \tag{41}$$

The easy way to derive an expression for the ratio of functional determinants is to use the formalism of Gel'fand and Yaglom [55], see also [42,49]. Within the latter, given a Schödinger operator defined on the interval $t \in [-\frac{\beta}{2}, \frac{\beta}{2}]$ with eigenfunctions satisfying Dirichlet[9] boundary conditions

$$\begin{aligned} L\psi(t) &= [-\partial_t^2 + U(t)]\psi(t) = k^2\psi(t), \\ \psi\left(-\frac{\beta}{2}\right) &= \psi\left(\frac{\beta}{2}\right) = 0, \end{aligned} \tag{42}$$

its determinant is found as a solution of the auxiliary problem

$$[-\partial_t^2 + U(t)]\phi(t) = 0, \quad \phi\left(-\frac{\beta}{2}\right) = 0, \quad \dot{\phi}\left(-\frac{\beta}{2}\right) = 1, \tag{43}$$

so that

$$\det[-\partial_t^2 + U(t)] = \phi\left(\frac{\beta}{2}\right). \tag{44}$$

In general, the above determinants diverge, so one generally considers their ratio

$$\frac{\det L_1}{\det L_2} = \frac{\phi_1(\frac{\beta}{2})}{\phi_2(\frac{\beta}{2})}. \tag{45}$$

This result could be straightforwardly obtained using the contour integration technique of Kirsten and McKane [56,57]. Indeed, writing the eigenvalue problem as

$$(L_j - k^2)u_{j,k}(t) = 0, \quad u_{j,k}\left(-\frac{\beta}{2}\right) = 0, \quad \dot{u}_{j,k}\left(-\frac{\beta}{2}\right) = 1 \tag{46}$$

and noting that if $u_{j,k}(t)$ satisfies the Dirichlet boundary conditions on both sides of the interval, i.e., if also

$$u_{j,k}\left(\frac{\beta}{2}\right) = 0, \tag{47}$$

then k^2 becomes the eigenvalue of L_j, and the sum of chosen powers of all eigenvalues of the latter could be conveniently represented by the following contour integral

$$\zeta_{L_j}(s) = \sum_{n=1}^{\infty} \frac{1}{k_n^{2s}} = \frac{1}{2\pi i} \int_\gamma k^{-2s} \frac{d}{dk} \ln u_{j,k}\left(\frac{\beta}{2}\right) dk, \tag{48}$$

[8]See for example [42,44].

[9]In the zero temperature case considered here, it is enough to consider Dirichlet boundary conditions.

where the contour runs counterclockwise and we used the fact that in the vicinity of the eigenvalue k_n

$$\frac{d}{dk}\ln u_{j,k}\left(\frac{\beta}{2}\right) \approx \frac{1}{k-k_n}. \tag{49}$$

The logarithmic derivative converges[10] as $|k| \to \infty$, and the integration contour could be deformed as we wish. Deforming the latter to imaginary axis we get

$$\zeta_{L_1}(s) - \zeta_{L_2}(s) = \frac{\sin(\pi s)}{\pi}\int_0^\infty k^{-2s}\frac{d}{dk}\ln\frac{u_{1,ik}(\frac{\beta}{2})}{u_{2,ik}(\frac{\beta}{2})}dk. \tag{50}$$

Recalling now that the operator determinants could be expressed as exponentials of the introduced zeta functions derivatives at zero, the determinant ratio is given by

$$\frac{\det L_1}{\det L_2} = e^{\zeta'_{L_2}(0)-\zeta'_{L_1}(0)} = \frac{u_{1,0}(\frac{\beta}{2})}{u_{2,0}(\frac{\beta}{2})}. \tag{51}$$

The presented derivation is valid if the considered operators do not contain zero modes. In our case, L_1 does actually have a zero mode due to the time translation invariance, and the above contour deformation is ill defined as $u_{1,k}(\frac{\beta}{2})$ is zero at $k=0$. To overcome this difficulty, we need to know the behavior of $u_{1,k}(\frac{\beta}{2})$ for small k to eliminate the pole in the integrand. Integrating by parts, the left-hand side of

$$\int_{-\frac{\beta}{2}}^{\frac{\beta}{2}} dt u_{1,0}(t)^* L_1 u_{1,k}(t) = k^2\int_{-\frac{\beta}{2}}^{\frac{\beta}{2}} dt u_{1,0}(t)^* u_{1,k}(t) \equiv k^2\langle u_{1,0}|u_{1,k}\rangle \tag{52}$$

gives

$$[\dot u_{1,0}(t)^* u_{1,k}(t) - \dot u_{1,k}(t)^* u_{1,0}(t)]_{-\frac{\beta}{2}}^{\frac{\beta}{2}} + \int_{-\frac{\beta}{2}}^{\frac{\beta}{2}} dt u_{1,k}(t)(L_1 u_{1,0}(t))^* = k^2\langle u_{1,0}|u_{1,k}\rangle. \tag{53}$$

Using the boundary conditions for $u_{1,0}(t)$ and $u_{1,k}(t)$, we get[11]

$$u_{1,k}\left(\frac{\beta}{2}\right) = \frac{k^2\langle u_{1,0}|u_{1,k}\rangle}{\dot u_{1,0}(\frac{\beta}{2})} \equiv -k^2 f_{1,k}. \tag{54}$$

It is easy to see that due to the orthogonality of the eigenfunctions, $f_{1,k}$ vanishes for all values of k^2 except at $k=0$, where it remains nonzero. A function which behaves as $u_{1,k}(\frac{\beta}{2})$ for large k but is nonzero for $k=0$ is given by $(1-k^2)f_{1,k}$, so the contour integral associated with the determinant of L_1 is given by

$$\frac{1}{2\pi i}\int_\gamma k^{-2s}\frac{d}{dk}\ln(1-k^2)f_{1,k}dk = \zeta_{L_1}(s) + \frac{1}{2\pi i}\int_\gamma k^{-2s}\frac{d}{dk}\ln(1-k^2)dk, \tag{55}$$

where the zero mode from $\zeta_{L_1}(s)$ was omitted. The second integral on the right-hand side is easily taken by a residue at simple pole $k=1$ and we get

$$\zeta_{L_1}(s) - \zeta_{L_2}(s) = \frac{\sin(\pi s)}{\pi}\int_0^\infty k^{-2s}\frac{d}{dk}\ln\left[\frac{(1+k^2)f_{1,ik}}{u_{2,ik}(\frac{\beta}{2})}\right] - 1. \tag{56}$$

The expression for the corresponding determinant ratio is then given by

$$\frac{\det' L_1}{\det L_2} = e^{\zeta'_{L_2}(0)-\zeta'_{L_1}(0)} = \frac{f_{1,0}}{u_{2,0}(\frac{\beta}{2})} = -\frac{\langle u_{1,0}|u_{1,0}\rangle}{\dot u_{1,0}(\frac{\beta}{2})u_{2,0}(\frac{\beta}{2})}, \tag{57}$$

where $\det'$ denotes the determinant with the zero eigenvalue omitted. The expression for the $u_{1,0}(x)$ function in the case of the functional determinant around the bounce solution could be easily found using the methods presented in the previous section and is given by

$$u_{1,0}(t) = \dot q_b(-\beta/2)\dot q_b(t)\int_{-\frac{\beta}{2}}^{t}\frac{dt'}{(\dot q_b(t'))^2}. \tag{58}$$

Here, we assumed that the parameter t_0 of the bounce solution was chosen, so that $\ddot q_b(-\frac{\beta}{2}) = 0$. This result could be easily generalized for more complicated boundary conditions, both with and without zero modes [56,57]. Finally, in our particular case we get

$$\lim_{\beta\to\infty}\frac{\det' L_b}{\det L_{FV}} = \lim_{\beta\to\infty}\frac{\det' \mathbb{D}}{\det \mathbb{D}_{FV}} = -\frac{(1-r^2)^2}{32r^7B^5M^{3/2}}S_b, \tag{59}$$

so that the imaginary part of energy is given by

$$\mathrm{Im}E = \frac{2AB}{B-A}\frac{M^{3/4}A^{3/4}B^{3/4}}{\sqrt{\pi}}e^{-S_b}. \tag{60}$$

We have checked that the same expression is reproduced using the formula presented in [50,51]. Moreover, it could also be obtained using slight modification of the derivation presented in [42] for the case of $U''(0) = \omega^2 \neq 1$. The above determinant ratio in this case is given by

[10] At large k, the potential in the Scrödinger operator could be neglected and we have $u_{j,k} \approx \sin(kx)[1+\mathcal{O}(k^{-1})]$.

[11] We dropped the $*$ as we are dealing with real solutions only.

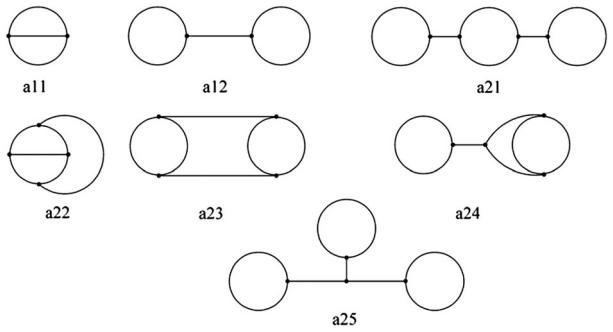

FIG. 5. Two and three loop Feynman diagrams with only cubic interaction vertexes.

$$\lim_{\beta\to\infty}\frac{\det'\mathbb{D}}{\det\mathbb{D}_{FV}}=-\frac{S_b}{2\omega q_0^2}\exp\left(-2\int_0^{q_0}dx\left[\frac{\omega}{\sqrt{2V(x)}}-\frac{1}{x}\right]\right), \tag{61}$$

where q_0 is the zero of potential and the turning point for the bounce solution. In our case, $q_0 = A$. The corresponding imaginary part of energy is then found with

$$\mathrm{Im}E=\frac{\omega^{\frac{3}{2}}q_0}{2\sqrt{\pi}}\exp\left(\int_0^{q_0}dx\left[\frac{\omega}{\sqrt{2V(x)}}-\frac{1}{x}\right]\right)e^{-S_b} \tag{62}$$

C. Non-Gaussian effects

To calculate higher order corrections, we are following [61–65] and use the Feynman diagram technique on top of the false vacuum and bounce solution. The first is used to calculate higher order contributions to the real part of the thermal partition function, while the latter is for higher order radiative corrections to its imaginary part. The corresponding Feynman rules are easy to derive and they are given by

$$\begin{aligned}
&V_{3,FV}=3M(A+B), \qquad V_{4,FV}=-12M,\\
&V_{3,b}=3M\left(A+B-\frac{4AB(1-x^2)}{B-Ax^2}\right), \qquad V_{4,b}=-12M,\\
&V_{\mathrm{tad}}=\frac{A^2(A-B)B^2M(1-x^2)(B-3(B-A)x^2-Ax^4)}{2S_b(Ax^2-B)^3}.
\end{aligned} \tag{63}$$

Note, that Feynman diagrams on top of bounce solution may contain single tadpole vertex coming from the Jacobian of transition to collective coordinate (19). Such diagrams appear only for the expansion on top of the bounce solution and are absent in the case of a false vacuum. The Green functions for the cases of the false vacuum and bounce solution were given in the previous subsection. Figures 5, 6, and 7 contain two and three loop diagrams containing only cubic vertexes, tadpole vertexes, and extra quartic vertexes, correspondingly. The diagram expressions, with account for symmetry factors, are constructed as how they usually done in quantum field theory. For example, the expression for the Feynman diagram $b22$ (see Fig. 6) is given by:

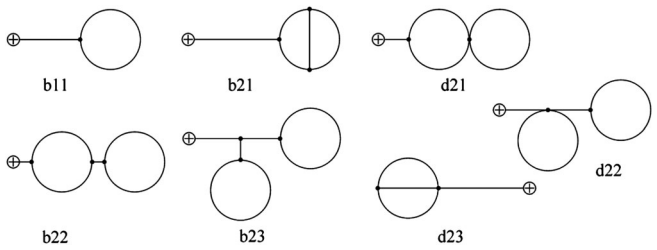

FIG. 6. Two and three loop Feynman diagrams with tadpole vertexes.

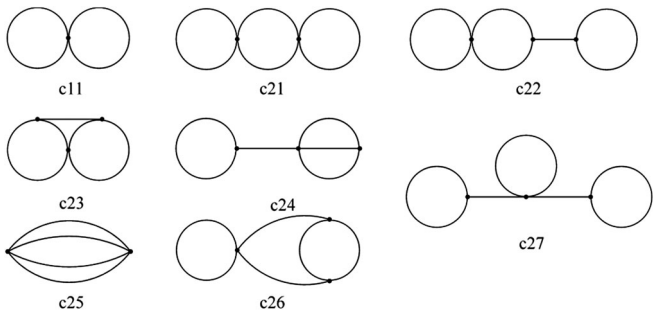

FIG. 7. Two and three loop Feynman diagrams with quartic in addition to cubic interaction.

$$\begin{aligned}
I_{b22}=&\frac{1}{4}\int_{-1}^{1}dx\int_{-1}^{1}dy\int_{-1}^{1}dz\int_{-1}^{1}dwJ_4V_{tad}(x)V_{3,b}(y)\\
&\times V_{3,b}(z)V_{3,b}(w)G(x,y)G^2(y,z)G(z,w)G(w,w),
\end{aligned} \tag{64}$$

where $J_n=\prod_{i=1}^{n}2/(1-x_i^2)$ is the Jacobian of transition from $t_1, t_2, \ldots t_n$ to $x, y, \ldots, w$ variables.

Diagrams without tadpole vertexes are present both in corrections to real and imaginary parts of thermal partition function. As the imaginary part of energy, what we are interested in is defined by their ratio, and it is convenient to combine these contributions, so that for example, the difference of the corresponding diagrams $c24$ for the bounce and false vacuum solutions is given by:

$$\begin{aligned}
I_{c24}=&\frac{1}{12}\int_{-1}^{1}dx\int_{-1}^{1}dy\int_{-1}^{1}dzJ_3(V_{3,b}(x)V_{4,b}(y)V_{3,b}(z)G(x,x)G(x,y)G^3(y,z)\\
&-V_{3,FV}(x)V_{4,FV}(y)V_{3,FV}(z)G_{FV}(x,x)G_{FV}(x,y)G_{FV}^3(y,z)).
\end{aligned} \tag{65}$$

To calculate two and three loop corrections to the false vacuum decay rate for arbitrary values of parameters A, B, M, one may use the mathematica notebook accompanying this article, where required numerical integrations are performed with the help of CUBA library [72]. Here we will only present the results for two particular cases used throughout this paper. In the limit $b \to 0$, the imaginary part of energy up to a three-loop accuracy is given by

$$\mathrm{Im}E = \frac{2AB}{B-A}\frac{M^{3/4}A^{3/4}B^{3/4}}{\sqrt{\pi}}e^{-S_b}\left\{1+\frac{I_2^0+\frac{b}{a^2}I_2^1+O(\frac{b^2}{a^4})}{S_b}+\frac{I_3^0+\frac{b}{a^2}I_3^1+O(\frac{b^2}{a^4})}{S_b^2}+\mathcal{O}(1/S_b^3)\right\}, \tag{66}$$

where in this case, $S_b = \frac{6}{5a^2}+\frac{4131}{560}\frac{b}{a^4}+\mathcal{O}(b^2)$ and I_2^i are two loop and I_3^i—three loop contributions (see Tables I and II)

$$I_2^0 = I_{a11}^0 + I_{a12}^0 + I_{b11}^0,$$
$$I_3^0 = \sum_{k=1}^{5} I_{a2k}^0 + \sum_{k=1}^{3} I_{b2k}^0 + I_{2\mathrm{contr}}^0, \tag{67}$$

with

$$I_{2\mathrm{contr}}^0 = \frac{1}{2}(I_{a11}^0 + I_{a12}^0)^2 + I_{b11}^0(I_{a11}^0 + I_{a12}^0) \approx 0.106 \tag{68}$$

TABLE I. Contributions of all two ant three loop diagrams in the case of $U(q) = \frac{1}{2}q^2 + \frac{a}{3}q^3$, potential. Here, s is the symmetry factor, i—diagram label and I_i—the diagram numerical value with absolute error ($b11$ is calculated exactly).

i	s	I_i^0
a11	1/12	$-0.162143 \pm 1.97 \times 10^{-6}$
a12	1/8	$0.0847623 \pm 7.32 \times 10^{-6}$
b11	1/2	$-559/420$
a21	1/16	$0.4497 \pm 1.5 \times 10^{-4}$
a22	1/24	$-0.01245 \pm 1.5 \times 10^{-5}$
a23	1/16	$0.100874 \pm 4 \times 10^{-5}$
a24	1/8	$0.03801 \pm 1.6 \times 10^{-4}$
a25	1/48	0.3942 ± 0.0042
b21	1/4	$-0.4297 \pm 6.2 \times 10^{-4}$
b22	1/4	$-0.9156 \pm 1.2 \times 10^{-4}$
b23	1/8	-1.2745 ± 0.0016

TABLE II. Linear in b corrections to all two-loop diagram contributions in the case of $U(q) = \frac{1}{2}q^2 + \frac{a}{3}q^3 + \frac{b}{4}q^4$ potential. Here, s is the symmetry factor, i—diagram label, and I_i—the diagram numerical value with absolute error ($c11$ is calculated exactly).

i	s	I_i^1
a11	1/12	$-0.748447 \pm 1.5 \times 10^{-5}$
a12	1/8	$-0.981144 \pm 4.8 \times 10^{-5}$
b11	1/2	$-8.338409 \pm 1.2 \times 10^{-5}$
c11	1/8	$6159/15400$

and

$$I_2^0 = -1.4083307 \pm 7.58 \times 10^{-6},$$
$$I_2^1 = -9.66805 \pm 5.2 \times 10^{-5},$$
$$I_3^0 = -1.543 \pm 0.0045.$$

In the case of $M = 1$, $A = 4$, $B = 8$, the corresponding corrections are given by (see Tables III and IV for the contributions of individual diagrams):

TABLE III. Two loop contributions for the case $M = 1$, $A = 4$, $B = 8$

i	s	I_i/S_b
a11	1/12	$-0.0023081 \pm 1.1 \times 10^{-6}$
a12	1/8	$-0.0310804 \pm 2.5 \times 10^{-6}$
b11	1/2	$-0.0365297 \pm 1.6 \times 10^{-6}$
c11	1/8	$0.00692251 \pm 1.8 \times 10^{-7}$

TABLE IV. Three loop contributions for the case $M = 1$, $A = 4$, $B = 8$. Here $I_{2loop} = \frac{1}{2}(I_{a11} + I_{a12} + I_{c11})^2 + I_{b11}(I_{a11} + I_{a12} + I_{c11})$

i	s	I_i/S_b^2
a21	1/16	$0.0000995 \pm 2.2 \times 10^{-6}$
a22	1/24	$-0.00001402 \pm 2.3 \times 10^{-7}$
a23	1/16	$0.00012921 \pm 6.1 \times 10^{-7}$
a24	1/8	$0.0000343 \pm 2.5 \times 10^{-6}$
a25	1/48	$-0.0000647 \pm 1.1 \times 10^{-6}$
c21	1/16	$-0.000037825 \pm 9 \times 10^{-9}$
c22	1/8	$0.00010217 \pm 5 \times 10^{-7}$
c23	1/8	$-0.0002733 \pm 3 \times 10^{-7}$
c24	1/12	$-0.00031362 \pm 3.8 \times 10^{-7}$
c25	1/48	$0.00018471 \pm 1 \times 10^{-8}$
c26	1/8	$-0.00009389 \pm 2 \times 10^{-7}$
c27	1/16	$0.00020214 \pm 2.6 \times 10^{-7}$
b21	1/4	$-0.0007047 \pm 1.1 \times 10^{-6}$
b22	1/4	$-0.0014675 \pm 1.6 \times 10^{-6}$
b23	1/8	$-0.0011163 \pm 2.2 \times 10^{-6}$
d21	1/4	$0.0003165 \pm 4.2 \times 10^{-7}$
d22	1/4	$0.00086871 \pm 2.9 \times 10^{-7}$
d23	1/6	$0.00029151 \pm 2.4 \times 10^{-7}$
I_{2loop}/S_b^2	-	$0.00131702 \pm 1.1 \times 10^{-7}$

$$\mathrm{Im}E = \frac{2M^{3/4}A^{7/4}B^{7/4}}{\sqrt{\pi}(B-A)}e^{-S_b}\left(1+\frac{I_2}{S_b}+\frac{I_3}{S_b^2}\right), \quad (69)$$

where

$$I_2/S_b = -0.0629957 \pm 3.2 \times 10^{-6}, \quad (70)$$

and

$$I_3/S_b^2 = -0.0005401 \pm 4.7 \times 10^{-6}, \quad (71)$$

We see that in the case with $M = 1$, $A = 4$, $B = 8$, the higher order corrections are small and could be safely neglected. On the other hand, in the limit $b \to 0$, the radiative corrections could be sizeable if $S_b \sim \mathcal{O}(1)$, and thus, should be taken into account.

III. CONCLUSION

In this paper, we considered the calculation of a false vacuum decay rate for the case of an arbitrary potential containing both cubic and quartic interactions in the framework of quantum mechanics. We obtained analytical expressions for both the Green functions in the background of bounce solutions as well as for a one-loop false vacuum decay rate. Besides, we provided numerical results for two and three-loop contributions to the decay rate together with a mathematica notebook, which could be used to evaluate two and three-loop radiative corrections for arbitrary values of cubic and quartic couplings. The presented techniques could be further generalized to the case of quantum field theory, which will be our next step.

ACKNOWLEDGMENTS

The authors would like to thank A. V. Bednyakov, A. E. Bolshov, M. Yu. Kalmykov, D. I. Kazakov, D. I. Melikhov, V. N. Velizhanin, O. L. Veretin, and A. F. Pikelner for interesting and stimulating discussions. This work was supported by RFBR Grants No. 17-02-00872, No. 16-02-00943 and Contract No. 02.A03.21.0003 from 27.08.2013 with Russian Ministry of Science and Education.

[1] G. Isidori, G. Ridolfi, and A. Strumia, On the metastability of the standard model vacuum, Nucl. Phys. **B609**, 387 (2001).
[2] Z. Lalak, M. Lewicki, and P. Olszewski, Higher-order scalar interactions and SM vacuum stability, J. High Energy Phys. 05 (2014) 119.
[3] A. D. Plascencia and C. Tamarit, Convexity, gauge-dependence and tunneling rates, J. High Energy Phys. 10 (2016) 099.
[4] M. Endo, T. Moroi, M. M. Nojiri, and Y. Shoji, Renormalization-Scale Uncertainty in the Decay Rate of False Vacuum, J. High Energy Phys. 01 (2016) 031.
[5] Z. Lalak, M. Lewicki, and P. Olszewski, Gauge fixing and renormalization scale independence of tunneling rate in Abelian Higgs model and in the standard model, Phys. Rev. D **94**, 085028 (2016).
[6] O. Czerwiska, Z. Lalak, M. Lewicki, and P. Olszewski, The impact of non-minimally coupled gravity on vacuum stability, J. High Energy Phys. 10 (2016) 004.
[7] J. R. Espinosa, M. Garny, T. Konstandin, and A. Riotto, Gauge-Independent Scales Related to the Standard Model Vacuum Instability, Phys. Rev. D **95**, 056004 (2017).
[8] M. Endo, T. Moroi, M. M. Nojiri, and Y. Shoji, On the Gauge Invariance of the Decay Rate of False Vacuum, Phys. Lett. B **771**, 281 (2017).
[9] M. Endo, T. Moroi, M. M. Nojiri, and Y. Shoji, False Vacuum Decay in Gauge Theory, arXiv:1704.03492.
[10] J. Elias-Miro, J. R. Espinosa, G. F. Giudice, G. Isidori, A. Riotto, and A. Strumia, Higgs mass implications on the stability of the electroweak vacuum, Phys. Lett. B **709**, 222 (2012).
[11] G. Degrassi, S. Di Vita, J. Elias-Miro, J. R. Espinosa, G. F. Giudice, G. Isidori, and A. Strumia, Higgs mass and vacuum stability in the Standard Model at NNLO, J. High Energy Phys. 08 (2012) 098.
[12] F. Bezrukov, M. Y. Kalmykov, B. A. Kniehl, and M. Shaposhnikov, Higgs Boson Mass and New Physics, J. High Energy Phys. 10 (2012) 140.
[13] S. Alekhin, A. Djouadi, and S. Moch, The top quark and Higgs boson masses and the stability of the electroweak vacuum, Phys. Lett. B **716**, 214 (2012).
[14] I. Masina, Higgs boson and top quark masses as tests of electroweak vacuum stability, Phys. Rev. D **87**, 053001 (2013).
[15] D. Buttazzo, G. Degrassi, P. P. Giardino, G. F. Giudice, F. Sala, A. Salvio, and A. Strumia, Investigating the near-criticality of the Higgs boson, J. High Energy Phys. 12 (2013) 089.
[16] J. R. Espinosa, G. F. Giudice, E. Morgante, A. Riotto, L. Senatore, A. Strumia, and N. Tetradis, The cosmological Higgstory of the vacuum instability, J. High Energy Phys. 09 (2015) 174.
[17] A. V. Bednyakov, B. A. Kniehl, A. F. Pikelner, and O. L. Veretin, Stability of the Electroweak Vacuum: Gauge Independence and Advanced Precision, Phys. Rev. Lett. **115**, 201802 (2015).
[18] E. Witten, Cosmic Separation of Phases, Phys. Rev. D **30**, 272 (1984).
[19] A. Kosowsky, M. S. Turner, and R. Watkins, Gravitational radiation from colliding vacuum bubbles, Phys. Rev. D **45**, 4514 (1992).

[20] A. Kosowsky, M. S. Turner, and R. Watkins, Gravitational waves from first order cosmological phase transitions, Phys. Rev. Lett. **69**, 2026 (1992).
[21] M. Kamionkowski, A. Kosowsky, and M. S. Turner, Gravitational radiation from first order phase transitions, Phys. Rev. D **49**, 2837 (1994).
[22] C. Caprini, R. Durrer, T. Konstandin, and G. Servant, General properties of the gravitational wave spectrum from phase transitions, Phys. Rev. D **79**, 083519 (2009).
[23] R. G. Cai, Z. Cao, Z. K. Guo, S. J. Wang, and T. Yang, The Gravitational Wave Physics, arXiv:1703.00187.
[24] A. D. Sakharov, Violation of *CP* Invariance, c Asymmetry, and Baryon Asymmetry of the Universe, Pis'ma Zh. Eksp. Teor. Fiz. **5**, 32 (1967) [JETP Lett. **5**, 24 (1967)]; A. D. SakharovUsp. Fiz. Nauk **161**, 61 (1991) [Sov. Phys. Usp. **34**, 392 (1991)].
[25] D. E. Morrissey and M. J. Ramsey-Musolf, Electroweak baryogenesis, New J. Phys. **14**, 125003 (2012).
[26] D. J. H. Chung, A. J. Long, and L. T. Wang, 125 GeV Higgs boson and electroweak phase transition model classes, Phys. Rev. D **87**, 023509 (2013).
[27] K. Kajantie, M. Laine, K. Rummukainen, and M. E. Shaposhnikov, Is there a hot electroweak phase transition at m(H) larger or equal to m(W)?, Phys. Rev. Lett. **77**, 2887 (1996).
[28] F. Csikor, Z. Fodor, and J. Heitger, Endpoint of the hot electroweak phase transition, Phys. Rev. Lett. **82**, 21 (1999).
[29] Y. Aoki, F. Csikor, Z. Fodor, and A. Ukawa, The Endpoint of the first order phase transition of the SU(2) gauge Higgs model on a four-dimensional isotropic lattice, Phys. Rev. D **60**, 013001 (1999).
[30] M. D'Onofrio and K. Rummukainen, Standard model cross-over on the lattice, Phys. Rev. D **93**, 025003 (2016).
[31] P. Burda, R. Gregory, and I. Moss, Gravity and the stability of the Higgs vacuum, Phys. Rev. Lett. **115**, 071303 (2015).
[32] P. Burda, R. Gregory, and I. Moss, Vacuum metastability with black holes, J. High Energy Phys. 08 (2015) 114.
[33] P. Burda, R. Gregory, and I. Moss, The fate of the Higgs vacuum, J. High Energy Phys. 06 (2016) 025.
[34] D. Gorbunov, D. Levkov, and A. Panin, Fatal youth of the Universe: black hole threat for the electroweak vacuum during preheating, arXiv:1704.05399.
[35] S. R. Coleman, The Fate of the False Vacuum. 1. Semiclassical Theory, Phys. Rev. D **15**, 2929 (1977); Erratum, Phys. Rev. D **16**, 1248(E) (1977).
[36] C. G. Callan, Jr. and S. R. Coleman, The Fate of the False Vacuum. 2. First Quantum Corrections, Phys. Rev. D **16**, 1762 (1977).
[37] S. Coleman and F. De Luccia, Gravitational effects on and of vacuum decay, Phys. Rev. D **21**, 3305 (1980).
[38] I. Y. Kobzarev, L. B. Okun, and M. B. Voloshin, Bubbles in Metastable Vacuum, Yad. Fiz. **20**, 1229 (1974) [Sov. J. Nucl. Phys. **20**, 644 (1975)].
[39] H. Kleinert, *Path Integrals in Quantum Mechanics, Statistics, Polymer Physics, and Financial Markets* (World Scientific, Singapore, 2004).
[40] H. J. W. Mller-Kirsten, *Introduction to Quantum Mechanics: Schrdinger Equation and Path Integral* (World Scientific, Hackensack, NJ, 2006).
[41] J. Zinn-Justin, Quantum field theory and critical phenomena, Int. ser. monogr. phys. **113**, 1 (2002).
[42] M. Marino, *Instantons and Large N: An Introduction to Non-Perturbative Methods in Quantum Field Theory* (Cambridge University Press, 2015).
[43] E. J. Weinberg, *Classical solutions in quantum field theory* (Cambridge Monographs on Mathematical Physics, 2012).
[44] A. Andreassen, D. Farhi, W. Frost, and M. D. Schwartz, Precision decay rate calculations in quantum field theory, Phys. Rev. D **95**, 085011 (2017).
[45] A. Andreassen, D. Farhi, W. Frost, and M. D. Schwartz, Direct Approach to Quantum Tunneling, Phys. Rev. Lett. **117**, 231601 (2016).
[46] D. V. Vassilevich, Heat kernel expansion: User's manual, Phys. Rep. **388**, 279 (2003).
[47] V. A. Novikov, M. A. Shifman, A. I. Vainshtein, and V. I. Zakharov, Calculations in External Fields in Quantum Chromodynamics. Technical Review, Fortschr. Phys. **32**, 585 (1984).
[48] O. K. Kwon, C. k. Lee, and H. Min, Massive field contributions to the QCD vacuum tunneling amplitude, Phys. Rev. D **62**, 114022 (2000).
[49] G. V. Dunne, Functional determinants in quantum field theory, J. Phys. A **41**, 304006 (2008).
[50] H. Kleinert and A. Chervyakov, Functional determinants via Wronski construction of Green functions, J. Math. Phys. (N.Y.) **40**, 6044 (1999).
[51] H. Kleinert and A. Chervyakov, Simple explicit formulas for Gaussian path integrals with time dependent frequencies, Phys. Lett. A **245**, 345 (1998).
[52] B. Garbrecht and P. Millington, Greens function method for handling radiative effects on false vacuum decay, Phys. Rev. D **91**, 105021 (2015).
[53] B. Garbrecht and P. Millington, Self-consistent solitons for vacuum decay in radiatively generated potentials, Phys. Rev. D **92**, 125022 (2015).
[54] B. Garbrecht and P. Millington, Self-consistent radiative corrections to false vacuum decay, arXiv:1703.05417.
[55] I. M. Gel'fand and A. M. Yaglom, Integration in Functional Spaces and its Applications in Quantum Physics, J. Math. Phys. (N.Y.) **1**, 48 (1960).
[56] K. Kirsten and A. J. McKane, Functional determinants by contour integration methods, Ann. Phys. (Berlin) **308**, 502 (2003).
[57] K. Kirsten and A. J. McKane, Functional determinants for general Sturm-Liouville problems, J. Phys. A **37**, 4649 (2004).
[58] A. I. Vainshtein, V. I. Zakharov, V. A. Novikov, and M. A. Shifman, ABC's of Instantons, Usp. Fiz. Nauk **136**, 553 (1982) [Sov. Phys. Usp. **25**, 195 (1982)].
[59] T. Schfer and E. V. Shuryak, Instantons in QCD, Rev. Mod. Phys. **70**, 323 (1998).
[60] S. Vandoren and P. van Nieuwenhuizen, Lectures on instantons, arXiv:0802.1862.
[61] A. A. Aleinikov and E. V. Shuryak, Instantons In Quantum Mechanics. Two Loop Effects. (in Russian), Yad. Fiz. **46**, 122 (1987).

[62] S. Olejnik, Do Nongaussian Effects Decrease Tunneling Probabilities? Three Loop Instanton Density For The Double Well Potential, Phys. Lett. B **221**, 372 (1989).
[63] M. A. Escobar-Ruiz, E. Shuryak, and A. V. Turbiner, Three-loop Correction to the Instanton Density. I. The Quartic Double Well Potential, Phys. Rev. D **92**, 025046 (2015); Erratum, Phys. Rev. D **92**, 089902(E) (2015).
[64] M. A. Escobar-Ruiz, E. Shuryak, and A. V. Turbiner, Three-loop Correction to the Instanton Density. II. The Sine-Gordon potential, Phys. Rev. D **92**, 025047 (2015).
[65] M. A. Escobar-Ruiz, E. Shuryak, and A. V. Turbiner, Quantum and thermal fluctuations in quantum mechanics and field theories from a new version of semiclassical theory, Phys. Rev. D **93**, 105039 (2016).
[66] G. V. Dunne and C. Schubert, Two loop selfdual Euler-Heisenberg Lagrangians. 1. Real part and helicity amplitudes, J. High Energy Phys. 08 (2002) 053.
[67] G. V. Dunne and C. Schubert, Two loop selfdual Euler-Heisenberg Lagrangians. 2. Imaginary part and Borel analysis, J. High Energy Phys. 06 (2002) 042.
[68] G. V. Dunne, in *From Fields to Strings: Circumnavigating Theoretical Physics*, edited by M. Shifman, A. Vainshtein, and J. Wheater (World Scientific, Singapore, 2005), Vol. 1, pp. 445–522.
[69] R. Roiban, A. Tirziu, and A. A. Tseytlin, Two-loop world-sheet corrections in $Ads_5 \times s^5$ superstring, J. High Energy Phys. 07 (2007) 056.
[70] R. Roiban and A. A. Tseytlin, Spinning superstrings at two loops: Strong-coupling corrections to dimensions of large-twist SYM operators, Phys. Rev. D **77**, 066006 (2008).
[71] See Supplemental Material at http://link.aps.org/supplemental/10.1103/PhysRevD.96.036001 for details.
[72] T. Hahn, CUBA: A Library for multidimensional numerical integration, Comput. Phys. Commun. **168**, 78 (2005).